ChemComm

COMMUNICATION

View Article Online
View Journal | View Issue

Cite this: *Chem. Commun.*, 2025, **61**, 14701

Received 21st May 2025,
Accepted 14th August 2025

DOI: 10.1039/d5cc02871j

rsc.li/chemcomm

Dual magnetic bistability with significant coercivity in a photo-responsive 1D Fe_2Fe cyanide chain

Ranjan Kharel, Sindhuja Joshi and Sanjit Konar *

A cyanide-bridged 1D Fe_2Fe chain exhibits rare dual magnetic bistability: thermal spin-crossover and light-induced single-chain magnet behaviour. Photoirradiation switches the system from a diamagnetic to a magnetically correlated paramagnetic state, featuring slow magnetic relaxation and a notably high coercive field of 0.52 T.

The molecules exhibiting bistable magnetic states have garnered significant attention owing to their potential use in high density molecular storage devices, switches and sensors.[1–7] Bistability in these molecular systems can be driven by magnetic anisotropy, spin-state transitions, long-range magnetic ordering, valence tautomerism, and/or electron transfer-coupled spin transition.[8–17] In molecular nanomagnets such as single-molecule magnets (SMMs) and single-chain magnets (SCMs), bistability typically stems from strong magnetic anisotropy and exchange interactions between metal centers, resulting in magnetic hysteresis.[18–22] In these systems, the magnetic polarization direction can reversibly change under an alternating external magnetic field.[23] In contrast, bistability in systems such as spin crossover (SCO) compounds, valence tautomers, and electron transfer-coupled spin transition (ETCST) complexes arises from changes in the spin state or magnetic coupling triggered by external stimuli such as temperature, light, or pressure.[15,24–28] Despite considerable progress in designing molecules with bistable magnetic states, a key challenge remains in achieving the rapid and reversible switching of these states for operations like writing and erasing data. A major breakthrough came with the discovery of the light-induced excited spin-state trapping (LIESST) effect in 1984, which demonstrated that spin-crossover (SCO) complexes could be switched between low-spin (LS) and photoexcited high-spin (HS*) states using specific wavelengths of light.[29] The reverse process (reverse-LIESST) also enables HS* to return to LS.[30,31] These transitions occur within picoseconds, offering fast and energy-efficient control over magnetic bistability.[32–34] The integration of spin-crossover (SCO) bistability into SCM systems to achieve external control over magnetic exchange and anisotropy has emerged as a promising strategy. This concept was successfully realized by Tao Liu and co-workers in 2013, where the light-triggered conversion of Fe^{2+} from a low-spin ($t_{2g}^6e_g^0$, $S = 0$) to a high-spin ($t_{2g}^4e_g^2$, $S = 2$) state in an octahedral coordination environment enabled reversible switching of both magnetic exchange interactions and magnetic anisotropy in cyanide-bridged 2D coordination polymers, resulting in photo-induced SCM behavior.[35] However, challenges in precisely tuning the ligand field strength to achieve both SCO and the LIESST effect have limited the number of reported SCO-based photo-switchable SCMs.[23,35,36] For an SCM, the total energy barrier (Δ_τ) for magnetization reversal arises from both the intrachain magnetic exchange interaction (Δ_ξ) and the magnetic anisotropy of the bridged metal ions (Δ_A), expressed as $\Delta_\tau = \Delta_\xi + \Delta_A$ for finite chains and $\Delta_\tau = 2\Delta_\xi + \Delta_A$ in the infinite chain limit.[20,37–39] In cyanide-bridged systems, strong magnetic exchange at low temperatures, combined with the anisotropy of Fe^{2+} high-spin centers, can give rise to SCM behavior. To confine exchange interactions along a single direction and suppress interchain coupling, pillar ligands are often employed to generate 2D sheets composed of magnetically isolated 1D chains.[35,40,41] However, connecting these chains may create rigid structures that can hinder complete thermal SCO, as the flexibility of the framework is crucial to accommodate the volume changes associated with spin-state transitions during SCO.[23] This rigidity might also prevent the LIESST effect and hence the photo-induced SCM behaviour. Moreover, connecting the chains can foster antiferromagnetic interchain interactions giving rise to metamagnetic behavior.[42]

In this vein, we report a cyanide bridged 1D Fe_2Fe chain obtained by bridging Fe^{II} ions using $[FeTp(CN)_3]^-$ units and a pendent ligand 2-(pyridin-4-yl)benzothiazole (L) to bind at the apical position of the Fe^{II} ion. The complex shows an abrupt thermal SCO behaviour, resulting in the electronic state change from $(Fe^{III}_{LS})_2Fe^{II}_{HS}$ (HS phase) at high temperature to $(Fe^{III}_{LS})_2Fe^{II}_{LS}$ (LS phase) at low temperature. Upon irradiation with light of 850 nm wavelength at 10 K, the LS phase could be photo-excited to the metastable HS* phase with the $(Fe^{III}_{LS})_2Fe^{II}_{HS}$ state. The

Department of Chemistry, Indian Institute of Science Education and Research Bhopal, Madhya Pradesh, 462066, India. E-mail: skonar@iiserb.ac.in

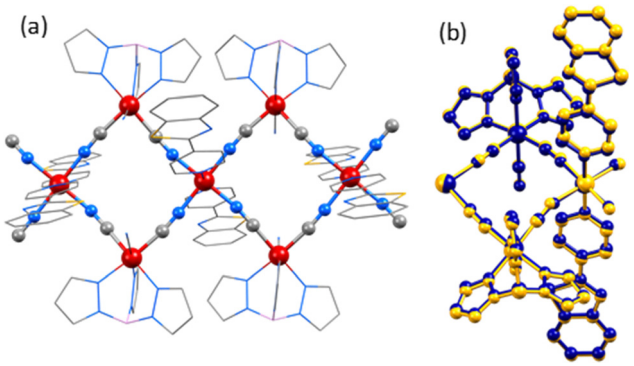

Fig. 1 (a) Crystal structure of the 1D chain, color code: orange (Fe), blue (N), grey (C). (b) Overlay diagram of the HS (yellow) and LS (blue) phases at 160 K and 100 K respectively.

generation of $(Fe^{III}_{LS})_2Fe^{II}_{HS}$ units in the chain ensures the switching of magnetic exchange interaction along with the anisotropy of the Fe^{II}_{HS} centres and hence the molecule exhibits SCM behaviour.

The single crystals of the target compound were obtained by slow evaporation of a methanol/water mixture of $Na[Fe(Tp)(CN)_3]$, 2-(pyridin-4-yl)-benzo-thiazole (L) and $Fe(ClO_4)_2{\cdot}6H_2O$. Single-crystal X-ray diffraction analysis showed that the compound crystallized in the orthorhombic space group *Pbcn* (Table S1, SI). The crystal structure consists of layered neutral mixed-valence $[Fe^{III}(Tp)(CN)_3]_2Fe^{II}(L)]$ units (Fig. 1a and Fig. S5–S7 and Table S2) without any solvent of crystallization as also confirmed by the TGA (Fig. S2). These layers, oriented in the ac plane and stacked along the *b* axis, contain cyanide-bridged $\{Fe^{III}_2Fe^{II}\}$ double-zigzag chains extending along the crystallographic *c* axis (Fig. S5–S7). The Fe2 centres adopt a distorted octahedral geometry and the six coordination sites are occupied by three N atoms from the Tp ligand and three C atoms of the cyanide groups. The two of the three cyanide groups of $[Fe^{III}(Tp)(CN)_3]^-$ units are bridged to two Fe1 centres, while the third one remains terminal. The Fe1 centre also adopts a distorted octahedral geometry with the N_6 configuration, comprising four N atoms from the cyanide groups and two from the ligand L. The $Fe–N_{cyanide}$ and $Fe–N_L$ of 2.117(3)–2.154(3) Å and 2.180(3) Å from the bond length analysis at 160 K indicated that the Fe1 centre is present in the Fe^{II}_{HS} state, while the Fe–C and Fe–N bond distances of 1.910(4)–1.927(4) Å and 1.966(3)–1.987(3) Å for the Fe2 centre are in the range for Fe^{III}_{LS} in the reported related systems.[23,35,43] Thus, the chain is comprised of $Fe^{III}_{LS}(\mu\text{-CN})Fe^{II}_{HS}$ linkages at 160 K. Upon decreasing the temperature to 100 K the $Fe–N_{cyanide}$ and $Fe–N_L$ bond lengths for the Fe1 centre decrease to 1.933(3)–1.956(3) Å and 1.997(2) Å, accompanied by a change in the unit cell volume by 3.13%, indicating the transformation of the $Fe1^{II}_{HS}$ to $Fe1^{II}_{LS}$ state. However, the bond distances around the Fe2 centres 1.915(3)–1.924(3) Å and 1.967(3)–1.983(3) Å do not undergo such variation, suggesting the formation of $Fe^{III}_{LS}(\mu\text{-CN})Fe^{II}_{LS}$ linkages in the chain. Thus, the variation of the temperature leads to the thermal SCO in the Fe1 sites. The overlay diagram for the structures at 100 K and 160 K clearly conveys the elongation/contraction of bonds during the SCO process (Fig. 1b). The increase of the octahedral distortion parameter Σ from 19.8° at 100 K to 25.1° at 160 K indicates a normal trend for SCO exhibiting molecules without elastic frustration (Table S3).[44,45] The interchain Fe1···Fe1 distances of 15.257 (3) Å at 100 K and 15.313(7) Å at 160 K indicate that the 1D chains are well separated. The IR data recorded at room temperature indicate ν_{CN} bands at 2122 cm^{-1}, 2142 cm^{-1} and 2151 cm^{-1}, assignable to the terminal and bridging cyanides of the $Fe^{III}_{LS}(\mu\text{-CN})Fe^{II}_{HS}(\mu\text{-CN})Fe^{III}_{LS}$ units (Fig. S1).

The magnetic susceptibility data for the complex (Fig. 2a) were collected under an applied magnetic field of 1000 Oe in both cooling (300–2 K) and heating (2–300 K) modes at a scan rate of 4 K min^{-1}. The phase purity of the bulk sample prior to the measurement was confirmed by PXRD (Fig. S4). At 300 K, the $\chi_M T$ value of 5.24 $cm^3\ mol^{-1}$ K is slightly higher than the calculated value of 4.99 $cm^3\ mol^{-1}$ K expected for one Fe^{II}_{HS} (S = 2, g = 2.2) and two Fe^{III}_{LS} (S = 1/2, g = 2.7) ions in an octahedral environment.[46,47] Upon cooling, the $\chi_M T$ value remained nearly constant down to 170 K, followed by a sharp decrease centered at $T_{1/2}$ = 152 K, eventually reaching 1.51 $cm^3\ mol^{-1}$ K at 50 K. This low temperature $\chi_M T$ value is consistent with the presence of one Fe^{II}_{LS} (S = 0) and two Fe^{III}_{LS} (S = 1/2, g = 2.7), with a calculated $\chi_M T$ value of 1.37 $cm^3\ mol^{-1}$ K. Upon increasing the temperature back from 2 to 300 K the $\chi_M T$ reaches the initial value with $T_{1/2}$ = 154 K. Thus, the Fe1 centre undergoes a reversible temperature induced SCO phenomenon. The reversible one-step SCO behaviour was also confirmed from the exothermic/endothermic peaks at ~151/153 K observed in the DSC analysis, performed with a sweep rate of 4 K min^{-1} (Fig. S3).

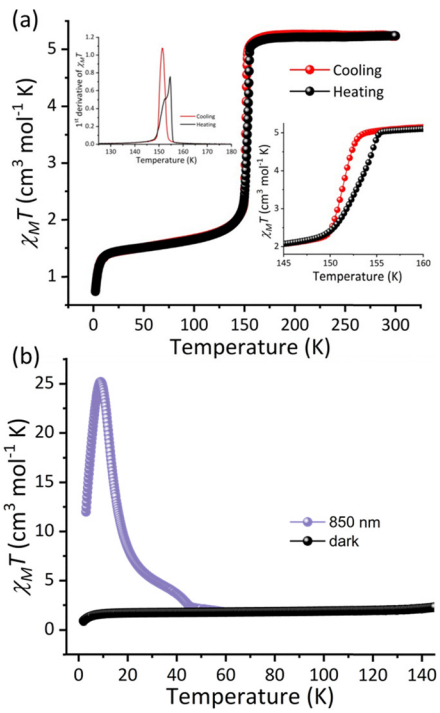

Fig. 2 (a) Temperature dependent magnetic susceptibility during cooling and heating cycles (inset: the first derivative plot and the zoomed-in view of the $\chi_M T$ *vs.* T plot). (b) Temperature dependent susceptibility after irradiation with 850 nm light.

To check the possibility of the LIESST phenomenon, photomagnetic studies were performed at 10 K under the irradiation with light of 850 nm wavelength. Upon irradiation the $\chi_M T$ value increased and almost reached saturation in about 5.3 hours (Fig. S10). After the photo-induced conversion, upon gradually increasing the temperature from 3 K the $\chi_M T$ value increased to a maximum of 25.17 $cm^3\ mol^{-1}$ K at 9 K consistent with ferromagnetic interaction between the Fe^{II}_{HS} ions ($S = 2$) and the Fe^{III}_{LS} ions ($S = 1/2$). As the temperature was gradually increased the diminishing influence of the magnetic exchange interaction resulted in the decrease of the $\chi_M T$ value to 5.24 $cm^3\ mol^{-1}$ K at 29 K and finally the Fe^{II}_{HS} state relaxed to Fe^{II}_{LS} above 50 K. The zero-field-cooled (ZFC) and field-cooled (FC) magnetisation data recorded at an applied field of 100 Oe after 850 nm irradiation indicates a bifurcation at around 4.8 K, indicating the blocking temperature and the onset of slow relaxation of magnetization (Fig. S11).[20,38,48] A hysteresis loop with a coercive field of 0.52 T at 1.8 K was obtained in the variable field magnetisation measurement, which is one of the highest among the reported photo-induced SCMs. Upon increasing the temperature to 3 K the coercive field decreases to 0.02 T, indicating faster magnetization dynamics with increase in temperature (Fig. 3).[20,23] The AC dynamic study before irradiation indicates no frequency dependency for both the in-phase (χ'_M) and out-of-phase (χ''_M) signals (Fig. S8 and S9); however after photo-irradiation with 850 nm light, the HS* phase indicates frequency dependency for both the χ'_M and χ''_M signals (Fig. 4a, b and Fig. S13, S14). The Mydosh parameter $\Phi = (\Delta T_P/T_P)/\Delta(\log(2\pi\nu))$ (where T_P is the peak temperature of the χ'' *vs.* T plot), which indicates the shift in the peak temperature, was calculated to be 0.17 and lies in the range of SCMs (*i.e.*, $0.1 \leq \Phi \leq 0.3$).[49] Based on the peak maxima of χ''_M, the relaxation times were extracted and fitted using the Arrhenius law, $\tau = \tau_0 \exp(\Delta_\tau/k_BT)$ (where $\tau = (2\pi\nu)^{-1}$), which yielded an overall energy barrier for the reversal of magnetization, $\Delta_\tau/k_B = 83$ K, and a preexponential factor, $\tau_0 = 5.3 \times 10^{-10}$ s (Fig. 4d). The obtained value of τ_0 agrees well with the values reported for photo-induced SCMs. The best fit of the Cole–Cole plot with a generalized Debye model in the temperature range of 4.4–5.2 K gave α values ranging from 0.33 to 0.41, indicative of wide distribution of relaxation times, possibly caused by weak interchain magnetic interactions/poly-dispersity of the chain length (Fig. S15).[48,50] Although the magnitude of χ''_M in the χ''_M *vs.* T plot decreased with decreasing frequency, we didn't observe any sharp peak in the variable field χ_M *vs.* T plot, indicating negligible interchain antiferromagnetic interactions (Fig. S12).[51,52] Variable temperature ac susceptibility data collected at zero applied dc field and an ac field of 3.5 Oe under an oscillation of 1 Hz were analysed using the equation $\chi'T = C_{eff}\exp(\Delta_\xi/k_BT)$ and the resulting effective Curie constant of C_{eff} = 1.77 $cm^3\ mol^{-1}$ K and the correlation energy of $\Delta_\xi/k_B = 30.10$ K were obtained (Fig. 4c). From the maxima of the $\chi'T$, the number of correlated units of $n = 45$ was estimated using the relation $[\chi'T]_{max} = nC_{eff}$. Therefore, the switching of the Fe^{II}_{LS} centres to Fe^{II}_{HS} centres upon irradiation turn on the magnetic exchange interaction along the 1D chain. The development of magnetic correlation coupled with the anisotropy of the Fe^{II}_{HS} centres results in the slow relaxation of magnetization and thus enables the realization of photo-induced SCM behaviour.

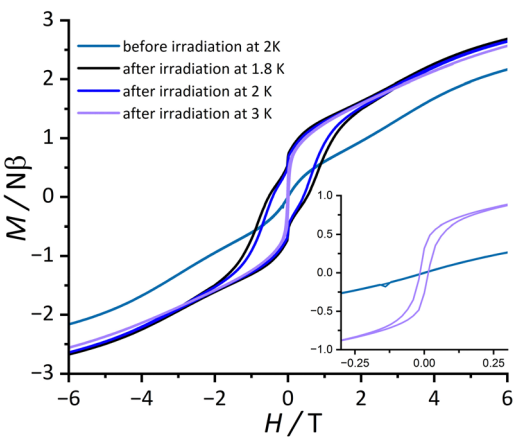

Fig. 3 Field dependent magnetization exhibiting hysteresis at different temperatures after photo-irradiation with 850 nm light.

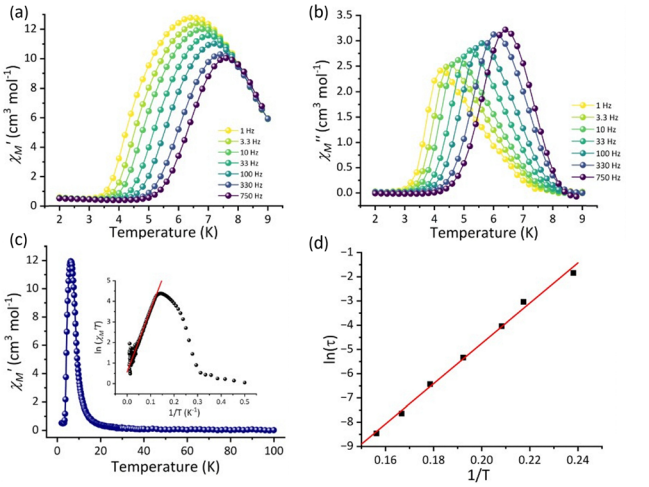

Fig. 4 AC susceptibility data collected under a 0 Oe applied dc field and a 3.5 Oe ac field oscillating at different frequencies after irradiation with 850 nm light. (a) In-phase (χ'_M) and (b) out-of-phase (χ''_M) ac susceptibility. (c) χ'_M collected at 1 Hz. Inset represents the plot of $\ln(\chi'T)$ *versus* T^{-1} (the red solid line indicates the best fit). (d) Plot of relaxation times *versus* T^{-1} (the red solid line indicates the best fit).

In summary, we report a cyanide-bridged 1D Fe_2Fe coordination polymer that exhibits dual magnetic bistability comprising spin-crossover (SCO) and photo-switchable single-chain magnet (SCM) behavior. The light-induced transformation of Fe^{II}_{LS} to Fe^{II}_{HS} in the Fe_2Fe chain activates intrachain magnetic exchange and anisotropy, enabling slow relaxation of magnetization. The molecule exhibits a significant coercive field of 0.52 T and an energy barrier for magnetization reversal of 83 K, placing it among the top-performing photo-induced SCMs reported to date. Our finding highlights the potential of combining SCO and SCM phenomena through the use of a pendant ligand to construct a 1D coordination polymer, effectively minimizing interchain interactions while maintaining flexibility for the development of responsive molecular magnetic materials.

R. K. acknowledges PMRF for the fellowship, S. J. thanks IISER Bhopal for the fellowship, and S. K. thanks SERB, India (Project no. CRG/2022/001676) and IISER Bhopal for financial, infrastructural, and instrumental support.

Conflicts of interest

There are no conflicts to declare.

Data availability

The datasets supporting this article have been uploaded as part of the SI. Supplementary information: Crystallographic and magnetic data, synthetic protocols, spectroscopic data, and related figures. see DOI: **https://doi.org/10.1039/d5cc02871j**

CCDC 2449302–2449304 contain the supplementary crystallographic data for this paper.[53–55]

Notes and references

1 O. Kahn and C. J. Martinez, *Science*, 1998, **279**, 44–48.
2 L. Bogani and W. Wernsdorfer, *Nat. Mater.*, 2008, **7**, 179–186.
3 G. Molnár, S. Rat, L. Salmon, W. Nicolazzi and A. Bousseksou, *Adv. Mater.*, 2018, **30**, 1703862.
4 L. Kipgen, M. Bernien, F. Tuczek and W. Kuch, *Adv. Mater.*, 2021, **33**, 2008141.
5 E. Coronado, *Nat. Rev. Mater.*, 2020, **5**, 87–104.
6 X. Xiao, Z.-J. Chen, R. J. Varley and C.-H. Li, *Smart Mol.*, 2024, **2**, e20230028.
7 I. C.-Y. Hou, L. Li, H. Zhang and P. Naumov, *Smart Mol.*, 2024, **2**, e20230031.
8 A. Paul, W. Kosaka, B. Kumar, D. J. Mondal, H. Miyasaka and S. Konar, *Chem. Sci.*, 2024, **15**, 15610–15616.
9 J. Yadav, D. J. Mondal and S. Konar, *Chem. Commun.*, 2021, **57**, 5925–5928.
10 J. Yadav and S. Konar, *Chem. Sci.*, 2025, **16**, 130–138.
11 J. M. Frost, K. L. M. Harriman and M. Murugesu, *Chem. Sci.*, 2016, **7**, 2470–2491.
12 D. Aguilà, Y. Prado, E. S. Koumousi, C. Mathonière and R. Clérac, *Chem. Soc. Rev.*, 2016, **45**, 203–224.
13 R. W. Hogue, S. Singh and S. Brooker, *Chem. Soc. Rev.*, 2018, **47**, 7303–7338.
14 J. T. Janetzki, D. S. Brown, F. Daumann, I. H. Ismail, R. W. Gable, M. A. Hay, R. J. Mulder, A. A. Starikova, B. Weber, M. J. Giansiracusa and C. Boskovic, *Chem. Sci.*, 2025, **16**, 5857–5871.
15 J. Yadav, R. Kharel and S. Konar, *Coord. Chem. Rev.*, 2025, **523**, 216283.
16 L. Sorace, A. A. Dmitriev, M. Perfetti and K. E. Vostrikova, *Chem. Sci.*, 2025, **16**, 218–232.
17 S.-Q. Wu, S.-Q. Su, S. Kanegawa and O. Sato, *Acc. Chem. Res.*, 2025, **58**, 1284–1295.
18 P. Kumar Sahu, R. Kharel, S. Shome, S. Goswami and S. Konar, *Coord. Chem. Rev.*, 2023, **475**, 214871.
19 C. A. Gould, K. R. McClain, D. Reta, J. G. C. Kragskow, D. A. Marchiori, E. Lachman, E.-S. Choi, J. G. Analytis, R. D. Britt, N. F. Chilton, B. G. Harvey and J. R. Long, *Science*, 2022, **375**, 198–202.
20 X. Liu, X. Feng, K. R. Meihaus, X. Meng, Y. Zhang, L. Li, J.-L. Liu, K. S. Pedersen, L. Keller, W. Shi, Y.-Q. Zhang, P. Cheng and J. R. Long, *Angew. Chem., Int. Ed.*, 2020, **59**, 10610–10618.
21 Y.-C. Chen and M.-L. Tong, *Chem. Sci.*, 2022, **13**, 8716–8726.
22 R. Kharel, J. Yadav and S. Konar, *Chem. Commun.*, 2024, **60**, 839–842.
23 L. Zhao, Y.-S. Meng, Q. Liu, O. Sato, Q. Shi, H. Oshio and T. Liu, *Nat. Chem.*, 2021, **13**, 698–704.
24 Y. Li, A. Benchohra, B. Xu, B. Baptiste, K. Béneut, P. Parisiades, L. Delbes, A. Soyer, K. Boukheddaden and R. Lescouëzec, *Angew. Chem., Int. Ed.*, 2020, **59**, 17272–17276.
25 Y. Zhang, D. Li, R. Clérac, M. Kalisz, C. Mathonière and S. M. Holmes, *Angew. Chem., Int. Ed.*, 2010, **49**, 3752–3756.
26 D. J. Mondal, N. Mukherjee and S. Konar, *Cryst. Growth Des.*, 2023, **23**, 1832–1839.
27 P. Sadhukhan, S.-Q. Wu, S. Kanegawa, S.-Q. Su, X. Zhang, T. Nakanishi, J. I. Long, K. Gao, R. Shimada, H. Okajima, A. Sakamoto, J. G. Chiappella, M. S. Huzan, T. Kroll, D. Sokaras, M. L. Baker and O. Sato, *Nat. Commun.*, 2023, **14**, 3394.
28 C. Lecourt, Y. Izumi, K. Maryunina, K. Inoue, N. Bélanger-Desmarais, C. Reber, C. Desroches and D. Luneau, *Chem. Commun.*, 2021, **57**, 2376–2379.
29 S. Decurtins, P. Gütlich, C. P. Köhler, H. Spiering and A. Hauser, *Chem. Phys. Lett.*, 1984, **105**, 1–4.
30 J.-F. Létard, P. Guionneau, L. Rabardel, J. A. K. Howard, A. E. Goeta, D. Chasseau and O. Kahn, *Inorg. Chem.*, 1998, **37**, 4432–4441.
31 Y.-C. Chen, Y. Meng, Y.-J. Dong, X.-W. Song, G.-Z. Huang, C.-L. Zhang, Z.-P. Ni, J. Navařík, O. Malina, R. Zbořil and M.-L. Tong, *Chem. Sci.*, 2020, **11**, 3281–3289.
32 M. Reinhard, K. Kunnus, K. Ledbetter, E. Biasin, D. B. Zederkof, R. Alonso-Mori, T. B. van Driel, S. Nelson, M. Kozina, O. J. Borkiewicz, M. Lorenc, M. Cammarata, E. Collet, D. Sokaras, A. A. Cordones and K. J. Gaffney, *ACS Nano*, 2024, **18**, 15468–15476.
33 G. Auböck and M. Chergui, *Nat. Chem.*, 2015, **7**, 629–633.
34 C. Sousa, C. de Graaf, A. Rudavskyi, R. Broer, J. Tatchen, M. Etinski and C. M. Marian, *Chem. – Eur. J.*, 2013, **19**, 17541–17551.
35 T. Liu, H. Zheng, S. Kang, Y. Shiota, S. Hayami, M. Mito, O. Sato, K. Yoshizawa, S. Kanegawa and C. Duan, *Nat. Commun.*, 2013, **4**, 2826.
36 Q. Liu, J.-X. Hu, Y.-S. Meng, W.-J. Jiang, J.-L. Wang, W. Wen, Q. Wu, H.-L. Zhu, L. Zhao and T. Liu, *Angew. Chem., Int. Ed.*, 2021, **60**, 10537–10541.
37 C. Coulon, V. Pianet, M. Urdampilleta and R. Clérac, in *Molecular Nanomagnets and Related Phenomena*, ed. S. Gao, Springer Berlin Heidelberg, Berlin, Heidelberg, 2015, pp. 143–184, DOI: **10.1007/430_2014_154**.
38 L. Shi, D. Shao, X.-Qs Wei, K. R. Dunbar and X.-Y. Wang, *Angew. Chem., Int. Ed.*, 2020, **59**, 10379–10384.
39 L. Bogani, A. Vindigni, R. Sessoli and D. Gatteschi, *J. Mater. Chem.*, 2008, **18**, 4750–4758.
40 J.-X. Hu, H.-L. Zhu, Y.-S. Meng, J. Pang, N. Li, T. Liu and X.-H. Bu, *CCS Chem.*, 2023, **5**, 865–875.
41 H.-Y. Sun, P.-D. Mao, F.-F. Yan, X.-F. Li, R.-H. Zhou, Y.-S. Meng and T. Liu, *Cryst. Growth Des.*, 2023, **23**, 7939–7946.
42 H. Zheng, Y.-S. Meng, G.-L. Zhou, C.-Y. Duan, O. Sato, S. Hayami, Y. Luo and T. Liu, *Angew. Chem., Int. Ed.*, 2018, **57**, 8468–8472.
43 D. J. Mondal, A. Mondal, A. Paul and S. Konar, *Inorg. Chem.*, 2022, **61**, 4572–4580.
44 G. Yang, S.-G. Wu, Z.-Y. Ruan, Y.-C. Chen, K.-P. Xie, Z.-P. Ni and M.-L. Tong, *Angew. Chem., Int. Ed.*, 2023, **62**, e202312685.
45 K.-P. Xie, Z.-Y. Ruan, B.-H. Lyu, X.-X. Chen, X.-W. Zhang, G.-Z. Huang, Y.-C. Chen, Z.-P. Ni and M.-L. Tong, *Angew. Chem., Int. Ed.*, 2021, **60**, 27144–27150.
46 A. Mondal, Y. Li, P. Herson, M. Seuleiman, M.-L. Boillot, E. Rivière, M. Julve, L. Rechignat, A. Bousseksou and R. Lescouëzec, *Chem. Commun.*, 2012, **48**, 5653–5655.
47 K. Mitsumoto, M. Ui, M. Nihei, H. Nishikawa and H. Oshio, *CrystEngComm*, 2010, **12**, 2697–2699.
48 Y.-Z. Zhang, B. S. Dolinar, S. Liu, A. J. Brown, X. Zhang, Z.-X. Wang and K. R. Dunbar, *Chem. Sci.*, 2018, **9**, 119–124.
49 Y. Aono, H. Yoshida, K. Katoh, B. K. Breedlove, K. Kagesawa and M. Yamashita, *Inorg. Chem.*, 2015, **54**, 7096–7102.
50 J. Yang, M.-L. You, S. Liu, Y.-F. Deng, X.-Y. Chang, S. M. Holmes and Y.-Z. Zhang, *Inorg. Chem.*, 2023, **62**, 17530–17536.
51 J.-H. Wang, M. K. Javed, J.-X. Li, Y.-Q. Zhang, Z.-Y. Li and M. Yamashita, *Dalton Trans.*, 2023, **52**, 15510–15517.
52 T. Liu, Y.-J. Zhang, S. Kanegawa and O. Sato, *J. Am. Chem. Soc.*, 2010, **132**, 8250–8251.
53 R. Kharel, S. Joshi and S. Konar, CCDC 2449302: Experimental Crystal Structure Determination, 2025, DOI: **10.5517/ccdc.csd.cc2n6prb**.
54 R. Kharel, S. Joshi and S. Konar, CCDC 2449303: Experimental Crystal Structure Determination, 2025, DOI: **10.5517/ccdc.csd.cc2n6psc**.
55 R. Kharel, S. Joshi and S. Konar, CCDC 2449304: Experimental Crystal Structure Determination, 2025, DOI: **10.5517/ccdc.csd.cc2n6ptd**.